Microphysical Processes Evident in Aerosol Forcing of Tropical Deep Convective Clouds

RACHEL L. STORER AND SUSAN C. VAN DEN HEEVER

Colorado State University, Fort Collins, Colorado

(Manuscript received 2 March 2012, in final form 4 September 2012)

ABSTRACT

This study investigates the effects of aerosols on tropical deep convective clouds (DCCs). A series of large-scale, two-dimensional cloud-resolving model simulations was completed, differing only in the concentration of aerosols available to act as cloud condensation nuclei (CCN). Polluted simulations contained more DCCs, wider storms, higher cloud tops, and more convective precipitation domainwide. Differences in warm cloud microphysics were largely consistent with the first and second aerosol indirect effects. The average surface precipitation produced in each DCC column decreased with increasing aerosol concentration. A detailed microphysical budget analysis showed that the reduction in collision and coalescence largely dominated the trend in average precipitation. The production of rain from ice, though it also decreased, became a more important contribution to precipitation as the aerosol concentration increased. The DCCs in polluted simulations contained more frequent extreme values of vertical velocity, but the average updraft speed decreased with increasing aerosols in DCCs above 6 km. An examination of the buoyancy term of the vertical velocity equation demonstrates that the drag associated with condensate loading is an important factor in determining the average updraft strength. The largest contributions to latent heating in DCCs were cloud nucleation and vapor deposition onto water and ice, but changes in latent heating were, on average, an order of magnitude smaller than those in the condensate loading term. The average updraft speed was largely affected by increased drag from condensate loading in more mature updrafts, while early storm updrafts experienced convective invigoration from increased latent heating.

1. Introduction

Tropical convection is a key component of the climate system, playing an important role in linking radiation, dynamics, and the hydrologic cycle in the atmosphere (Arakawa 2004). Deep tropical convection in particular is a significant source of precipitation (Haynes and Stephens 2007; Liu 2011), and acts to transport heat upward through the troposphere with vertical motions and the release of latent heat. In addition, the deep convective clouds that form in the tropics are necessary for the global circulation of the atmosphere, as they are the primary means by which energy is transported from the tropics to the midlatitudes (Riehl and Malkus 1958; Fierro et al. 2009, 2012).

The importance of convection to the climate system dictates that an effort be made to understand factors, environmental and otherwise, that can influence tropical convective clouds. The focus of this study is on aerosol indirect effects—a key uncertainty in our current and changing climate (Solomon et al. 2007). Particularly, the goal is to understand changes that can occur, to precipitation amount and storm strength, in tropical deep convective clouds because of an increase in the environmental concentration of aerosols (both natural and anthropogenic) that can act as cloud condensation nuclei (CCN). This study investigates these aerosol indirect effects on tropical deep convection utilizing a series of large-scale, high-resolution simulations using a radiative–convective equilibrium (RCE) framework. The simulations were performed using a cloud-resolving model (CRM) with detailed microphysics, and the budgets of various hydrometeors and microphysical processes were examined in order to point to the key changes impacting deep convection.

a. Tropical convection and radiative–convective equilibrium

It has been observed that tropical convection is typically organized in a trimodal distribution (Johnson et al.

Corresponding author address: Rachel L. Storer, Department of Atmospheric Science, Colorado State University, Fort Collins, CO 80523-1371.
E-mail: storer@atmos.colostate.edu

DOI: 10.1175/JAS-D-12-076.1

1999; Posselt et al. 2008), with the three peaks corresponding to shallow trade wind cumulus, cumulus congestus, and cumulonimbus clouds. This study is concerned with deep convective clouds (DCCs) that typically extend through the depth of the troposphere. In the tropics, DCCs are a ubiquitous feature that often organize into larger-scale structures such as squall lines (Rickenbach and Rutledge 1998). DCCs are also responsible for a significant portion of the rainfall in the tropics, particularly in the intertropical convergence zone (ITCZ) and the western Pacific warm pool region (Haynes and Stephens 2007). Liu (2011) showed that in many regions in the tropics, over 50% of the rainfall could be attributed to raining precipitation features with radar echo top heights above 10 km.

In this study, tropical DCCs are examined within the framework of RCE. A simple radiative equilibrium assumption leaves the atmosphere absolutely unstable to vertical motions. By allowing convection, latent and sensible heat can be transported vertically and released in the upper troposphere, removing this instability. Over a sufficiently long temporal integration, the modeled atmosphere relaxes to an equilibrium state, with a cooler surface and warmer upper troposphere than in the initial state. The vertical profiles of the atmosphere created in RCE simulations are quite similar to those that have been observed in the tropical atmosphere. Several studies (Held et al. 1993; Tompkins and Craig 1998; Bretherton et al. 2005; Grabowski 2006; Stephens et al. 2008; van den Heever et al. 2011) have successfully used the RCE framework to simulate the climate state of the tropics.

b. Aerosol indirect effects

The first and second aerosol indirect effects (Twomey 1977; Albrecht 1989) together explain the behavior of warm clouds in polluted environments—that is, environments with more aerosols available to act as CCN. In situations of equal liquid water content, polluted clouds will have more and smaller cloud droplets, higher albedos, and will produce less warm rain owing to a less efficient collision–coalescence process. While there can be some differences in these effects (both in magnitude and sign) due to cloud type (Seifert and Beheng 2006; van den Heever et al. 2011) and environment (Khain et al. 2008; Lebsock et al. 2008; Fan et al. 2009; Storer et al. 2010), many aspects of aerosol indirect effects on warm clouds are fairly well understood.

The addition of ice, however, leads to a much more complex response. In particular, the response of DCCs to aerosol forcing is currently not well understood. Throughout the warm cloud depth, these clouds appear to behave similarly to simple cumulus clouds or a stratocumulus deck—they have more, smaller cloud droplets and less efficient warm rain production (Rosenfeld and Lensky 1998; Khain et al. 2005; van den Heever et al. 2006; Rosenfeld et al. 2008; Storer et al. 2010; Tao et al. 2012). The consensus in previous work seems to indicate that DCCs formed in polluted environments will contain larger amounts of cloud water because of the suppressed warm rain process. It follows then that more ice will form as this additional cloud water is lofted above the freezing level. The increased ice amounts can then influence other important aspects of the storm. The formation of the increased ice amounts is postulated to lead to a larger latent heat release, which can enhance storm updrafts, thus producing convective invigoration (Andreae et al. 2004; Khain et al. 2005; van den Heever et al. 2006). Convective invigoration is likely to result in increased surface precipitation totals. Additionally, the presence of increased ice mass in polluted storms may lead to changes in the production of precipitation through melting processes. The combination of convective invigoration and the additional pathways for precipitation formation may lead to a precipitation gain that can counteract, or even overcome, the loss in warm rain, leading to a net increase in accumulated precipitation.

Several modeling (Khain et al. 2005; Wang 2005; van den Heever et al. 2006; Fan et al. 2007; van den Heever and Cotton 2007; Lee et al. 2008b) and observational (Andreae et al. 2004; Koren et al. 2010; Li et al. 2012) studies have found evidence of convective invigoration. However, Storer et al. (2010) did not see any evidence of supercell storm strength being affected by aerosols, and the question of invigoration or suppression of convection may strongly depend on the environment (Khain et al. 2008; Fan et al. 2009). The results were again mixed when concerning precipitation produced by deep convective storms in polluted environments. One study (Khain 2009) made an attempt to classify the effects of aerosols on deep convective precipitation by analyzing a number of previous studies in terms of a mass budget. The general trend found was that in polluted storms, there was an increase both in condensation and in condensate loss through the increase in evaporation with smaller cloud drops. They proposed that the net effect on precipitation could be found to depend on the difference in the changes of those two terms. Therefore, in studies of deep convection in dry environments the increase in condensate loss was greater than that of condensate gain and so precipitation was suppressed in polluted scenarios, whereas the reverse would occur in moist environments and an increase in precipitation could be found. Other recent studies have found that atmospheric stability (Storer et al. 2010) and shear (Fan

et al. 2009) can also act to modulate the effects of aerosols on precipitation in convective storms.

With all of the mixed results that have been found, it remains clear that while ice plays an important role in aerosol/convection interactions, the details are not currently well understood. It has been suggested that convective invigoration may be brought about by increases in latent heating due to the freezing of cloud water. However, this is not the only process acting in DCCs. Multiple processes involving phase changes (riming, melting, vapor deposition, etc.) all occur simultaneously, and it is not well known exactly how all of these processes interact to produce latent heat within convective clouds. Similar uncertainty exists surrounding the question of aerosol impacts on surface precipitation. Again, this is because there are multiple processes that act to form precipitation in DCCs (such as the melting of hail and other ice species in addition to the warm rain process). It is not currently known how aerosols affect all of these various processes, making the net effect of aerosols on surface precipitation difficult to predict.

In this study, the effects of aerosols on DCCs are examined within a series of large-scale, two-dimensional CRM simulations using an RCE framework. The RCE framework offers the ability to simulate a large-scale, idealized tropical atmosphere, including realistic cloud populations. The analysis presented concentrates on aerosol effects on DCCs, of which there are a large sample in each simulation. A detailed examination of the microphysics budget is undertaken in order to understand the processes important to convective invigoration and surface precipitation, and how these processes are affected by an increase in aerosols that can act as CCN.

2. Model description and experiment setup

The Regional Atmospheric Modeling System (RAMS) (Pielke et al. 1992; Cotton et al. 2003), version 6.0, was used for the simulations described here. RAMS is a limited area, nonhydrostatic, cloud-resolving model that utilizes a detailed two-moment microphysics scheme (Meyers et al. 1997). This microphysics scheme is considered bin emulating, as it has the reduced computational time of a bulk scheme, while using detailed lookup tables in order to capture aspects of a bin microphysics scheme. Lookup tables are previously generated offline for several important processes such as the activation of CCN (Saleeby and Cotton 2004), cloud drop collection (Feingold et al. 1988), and drop sedimentation (Feingold et al. 1998) through the use of a detailed parcel model. One important feature of the microphysics scheme in RAMS is the fact that CCN concentration is predicted based on background aerosol concentrations and environmental conditions, rather than being initially prescribed (Saleeby and Cotton 2004). Aerosols can be introduced into the model at any time, are advected throughout the model domain, and are lost through activation. A summary of model options utilized is included in Table 1.

TABLE 1. Model setup and parameterizations used in the simulations.

Model parameter	Setting
Model grid	Two-dimensional grid Horizontal: 7200-km domain, $\Delta x = 1$ km Vertical: 65 levels up to a 25-km model top, Δz variable 11 levels below 1 km AGL
Initialization	0000 UTC 5 Dec 1992 TOGA COARE sounding with zero mean wind Randomized perturbations to the potential temperature field
Time step	10 s
Duration of simulations	100 days (10 days after RCE analyzed)
Model physics	Nonhydrostatic, convection resolving
Microphysics	Two-moment bulk microphysics scheme (Meyers et al. 1997) Prognostic aerosol scheme (Saleeby and Cotton 2004)
Boundaries	Periodic lateral boundaries Rayleigh friction layer over top four model levels topped with a rigid lid Fixed model ocean surface, SST = 300 K
Radiation	Two-stream radiation scheme (Harrington et al. 1999)
Surface scheme	LEAF-2 (Walko et al. 2000)

The simulations performed for this study are similar to those described by van den Heever et al. (2011). The model was run using a two-dimensional domain in order to cover a large zonal extent (7200 km) with sufficiently fine model resolution. By utilizing such a domain, it is possible to look at a large sample of convective clouds forming in different conditions within the same RCE simulation. The solar zenith angle was held fixed at 50°, and hence the diurnal cycle is not included in the simulations. The model was run with a horizontal grid spacing of 1 km, so that convection was explicitly resolved. There were 65 levels in the vertical, with stretched spacing. The model was initialized with a sounding from the Tropical Ocean Global Atmosphere Coupled Ocean–Atmosphere Response Experiment (TOGA COARE) and zero mean wind. The aerosol concentration during the initial portion of the simulations was 25 cm^{-3} at the surface, decreasing with height. Random potential temperature perturbations were initially introduced into the boundary layer in order to initiate convection.

The simulation was run until RCE was achieved (60 days). At this point, the model was restarted with the introduction of various concentrations of aerosols that can serve as CCN. Aerosols were added in the 2–4-km layer and the concentration in this layer was reset each time step. This represents a continuous source of aerosols being advected into this layer. While aerosols were only introduced in a 2-km layer, they are advected through the whole domain, and many are available to be ingested into clouds in the boundary layer. The elevation of the aerosol layer is similar to the height of the Saharan dust events often seen in the tropical Atlantic (Carlson and Prospero 1972; Karyampudi et al. 1999). While African dust is typically considered for its role as ice nuclei (Demott et al. 2003), recent studies (Twohy et al. 2009) have shown that dust also can be effective as CCN or giant CCN (GCCN). In this study, the aerosols were only considered for their role as CCN in order to simplify the analysis of the interactions being investigated.

Six simulations were completed, identical except for the available aerosol concentration in the 2–4-km layer. The aerosol concentrations were doubled from a ''clean'' 100 cm^{-3} to a very polluted 3200 cm^{-3}. The high end of concentrations examined here is out of the range of what has ordinarily been measured for Saharan dust events. For example, Zipser et al. (2009) measured particle concentrations of 300–600 cm^{-3} in the National Aeronautics and Space Administration (NASA) African Monsoon Multidisciplinary Analysis (NAMMA) field campaign. However, similar concentrations have been measured in urban areas (Rose et al. 2010) and for an idealized study such as this, the goal was to examine the cloud process responses to a wide range of possible aerosol concentrations.

Ten days of simulation time were analyzed, and model output was sampled every 5 min throughout that time period. For the purposes of this study, a DCC was defined as a model column that contained cloud (cloud water + cloud ice > 0.01 g kg^{-1}) through a consecutive layer at least 8 km deep. The clouds studied include both single isolated deep convective towers and larger, organized cloud systems (though only in two dimensions). Additionally, the DCC profiles analyzed include all stages in the lifetime of a deep convective storm, both new growing convection and older, more mature convective profiles that meet the depth requirement. However, the depth of cloud required does ensure that the DCCs are likely to be part of the convective core. Most stratiform profiles would not meet the DCC requirements, as they would consist largely of precipitation (rain or hail, which are not included in the definition of cloud) in the low levels. As the domainwide changes in microphysical processes, and not the larger-scale storm organization, are the focus here, no attempt was made to separate aerosol effects based on storm type or stage of development. Unless otherwise noted, all of the fields analyzed here are averaged only over those model columns containing DCCs.

3. Results

a. Convective organization

Large-scale convective circulations set up within the model domain, with moist regions of rising motion and dry regions of subsidence, as typical within RCE simulations. There are two large (1000–2000 km wide) bands of moisture, similar to that shown in van den Heever et al. (2011), and the DCCs analyzed in this work fall within the moist regions. These large-scale simulations also capture a realistic arrangement of clouds, with a trimodal peak in cloud fraction similar to what has been seen previously (Johnson et al. 1999; Posselt et al. 2008).

Before narrowing down the analysis to DCC profiles only, it is useful to examine domainwide differences in organization brought about by changes in aerosol concentrations. Figure 1a shows the total number of profiles that qualified as DCCs for each simulation. As stated above, a DCC is defined as a column containing cloud (cloud water + cloud ice > 0.01 g kg^{-1}) through a continuous depth of at least 8 km. The DCCs examined are likely to be part of the core of deep convective storms owing to the fact that the depth requirement does not include precipitation hydrometeors in the definition. It is clear from this figure that more DCC profiles are present with increasing aerosol concentrations. The average width of the convective storms was calculated by simply counting consecutive DCC profiles across the horizontal domain. Figure 1b demonstrates that the average width of the deep convective storms is greater in polluted simulations; the total number of individual storms is also higher (not shown). Polluted simulations thus contain more deep convective storms that are larger in extent than in the cleaner scenarios, lending support to the hypothesis that aerosols invigorate convection. It is demonstrated in section 3b that the average precipitation produced by a DCC (calculated by averaging over all DCC columns) is lower in polluted simulations. However, the total precipitation produced by DCCs increases with increasing aerosols, since there are more storms (that are also larger and stronger) contributing to the total amount. Precipitation produced by other clouds shows a significant reduction with increasing aerosols [as demonstrated by van den Heever et al. (2011) and hence not shown here], likely as a consequence of

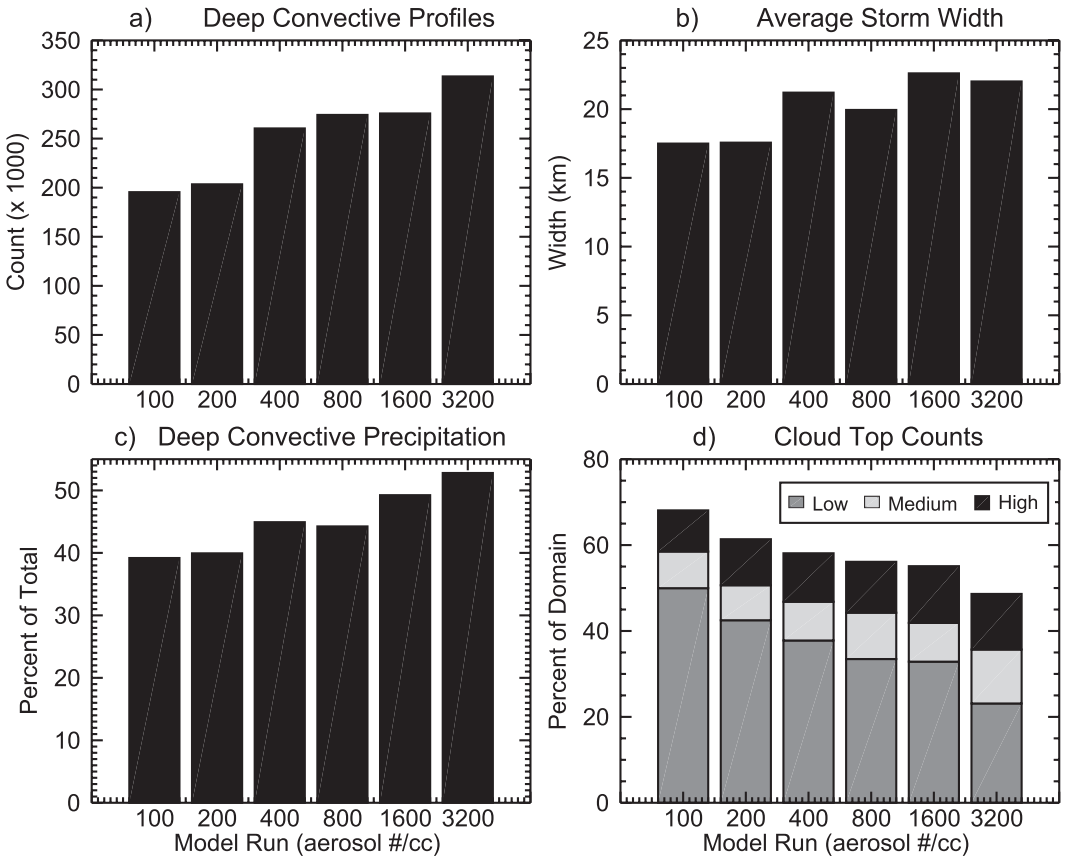

FIG. 1. Statistics over the whole model domain, for 10 days after RCE was reached: (a) total number of deep convective profiles analyzed for each simulation; (b) the average width of deep convective storms for each simulation; (c) convective precipitation, as a percentage of total domainwide precipitation; and (d) counts of cloud-top heights for each simulation, plotted as a percentage of the total domain. The cloud tops are split into low clouds [cloud top below the freezing level (about 4.4 km)], medium clouds (those with a cloud top between 4.4 and 10 km), and high clouds (cloud top above 10 km).

the second aerosol indirect effect and changes to the large-scale circulation, so the percentage contribution of deep convective storms to the total surface precipitation is much higher in polluted simulations (Fig. 1c), given their enhanced frequency.

The polluted simulations contain more deep convective storms that are broader and have higher cloud tops (not shown). The increase in convective mass flux in polluted scenarios must be compensated for elsewhere in the model domain. A simple illustration of this can be seen in Fig. 1d, showing the cloud-top counts over the whole model domain. It can be seen that while there is an increase in the number of high cloud tops, there is a substantial decrease in low clouds. The increased convective mass flux associated with convective invigoration is compensated by increased subsidence in the drier regions of the domain (van den Heever 2011), thus suppressing cloud formation in the trade wind cumulus regimes.

Increasing the number of aerosols available to act as CCN has definitive impacts on cloud organization and structure, as evidenced by the fact that polluted simulations contain more storms that are broader and deeper. The changes to the large-scale organization indicate that the convective circulation is being invigorated. There is more convective mass flux upward and stronger compensating subsidence in polluted simulations. In addition, the convective precipitation increases with increased aerosol concentrations, while the precipitation contribution from other cloud types, such as the trade wind cumulus clouds that would be found in subsidence regions, decreases.

b. Microphysics changes and precipitation response

Throughout the warm cloud depth of the DCCs examined here, the microphysical changes that occur in polluted simulations are similar to the aerosol indirect effects initially described for shallow clouds (Twomey

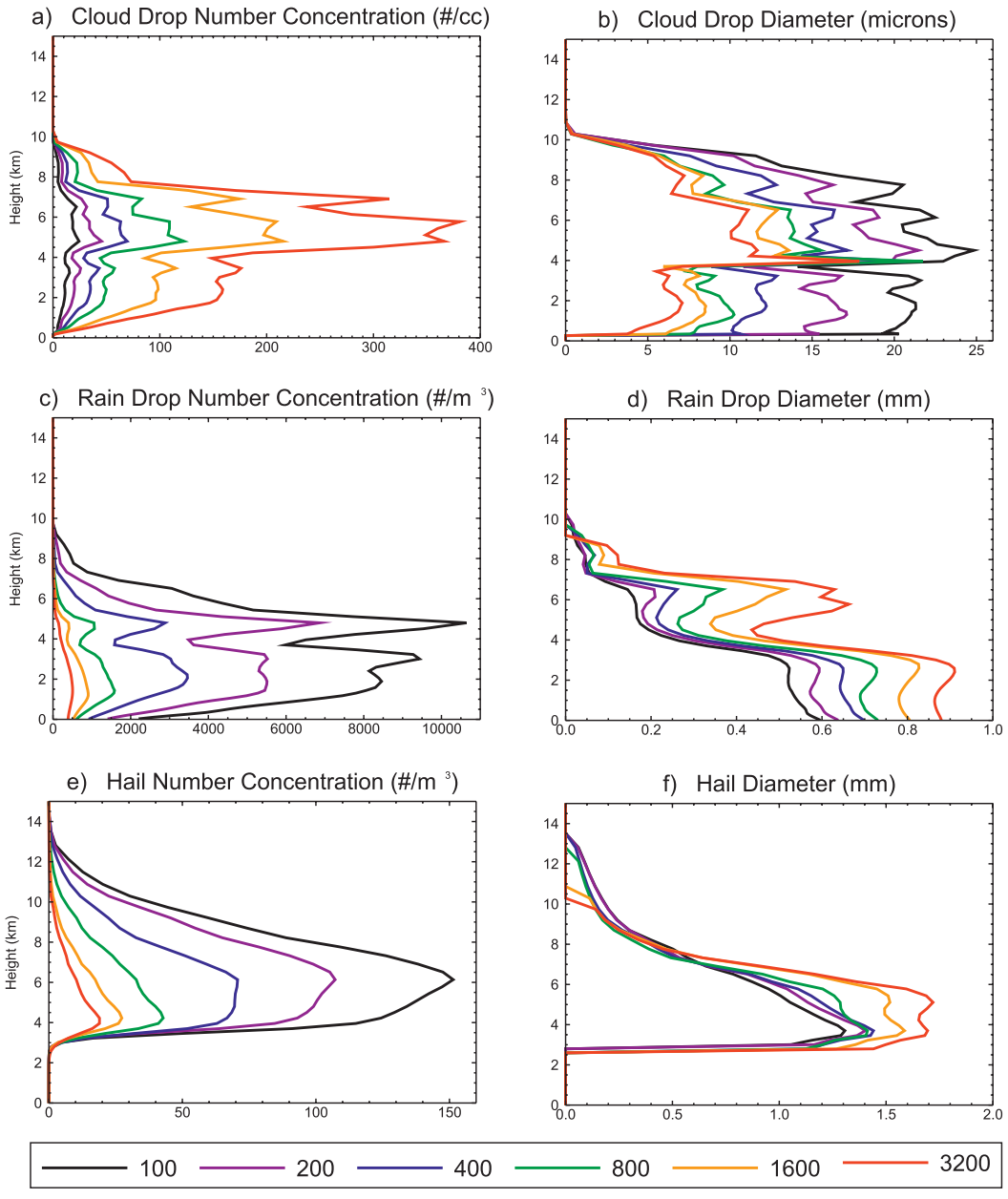

FIG. 2. (a),(c),(e) Mean number concentration and (b)(d),(f) the averaged mass-weighted mean diameter of (a),(b) cloud drops, (c),(d) raindrops, and (e),(f) hail, averaged over DCC profiles.

1977; Albrecht 1989). With more aerosols available to act as CCN, more cloud drops are formed in polluted simulations and drop sizes are smaller because of greater competition for water vapor (Fig. 2). The collision and coalescence process is therefore less efficient, owing to the narrower cloud droplet spectrum, and it becomes more difficult for raindrops to form. The reduced efficiency of warm rain production leads to a decrease in the mass of rain, and an increase in cloud water (Fig. 3). As shown in Fig. 2, the raindrops that do form are larger in polluted simulations. This is a combination of multiple effects. First, since autoconversion is suppressed in polluted storms, more cloud water is available for accretion once rain formation begins. Thus, the raindrops that form are able to grow faster as they fall, which can be seen by the more pronounced peak in raindrop size at around 6 km. Below the freezing level, there is another substantial peak in raindrop diameter as the melting of hail becomes an important process in rain production. Hailstones shed comparatively large raindrops, and as

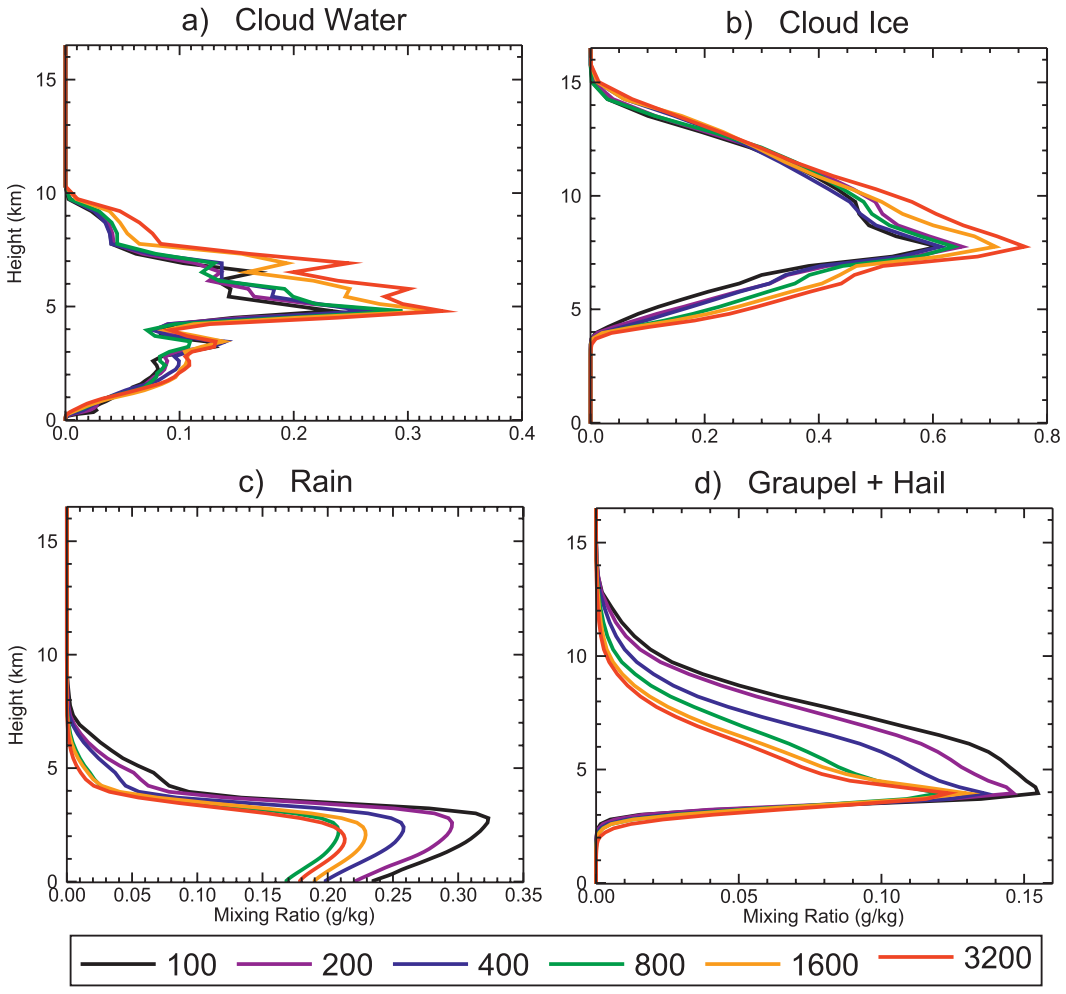

FIG. 3. Average profiles of mixing ratio for (a) cloud water, (b) cloud ice (pristine ice, snow, and aggregates), (c) rain, and (d) graupel and hail in DCC profiles.

hail size increases the number of drops shed will also increase. Thus, in polluted simulations there are more of these large drops contributing to the average raindrop size. The mean raindrop diameter also increases slightly below cloud as smaller drops will evaporate first. This increase in raindrop size with increasing aerosols is consistent both with previous model results (Altaratz et al. 2007; Berg et al. 2008; Storer et al. 2010) and observations (May et al. 2011).

The response of the ice hydrometeors to increased aerosol concentrations is similar to that of liquid water (Fig. 3), meaning there is less mass of precipitation-sized ice (graupel and hail), but an increase in the mass of smaller cloud ice hydrometeors in polluted storms. Because of the less-efficient warm rain process and increased amount of cloud water, more water can be lofted above the freezing level to produce ice. Thus, the mass of cloud ice (pristine, snow, and aggregates) increases for increased aerosol concentration. Graupel and hail show a decrease in mass similar to that of rain. These large, precipitation-sized ice particles form when an aggregate or snow flake becomes sufficiently rimed. Since there are more, smaller ice particles in polluted DCCs, there is greater competition for water, and it becomes more difficult for each particle to grow enough to become hail, leading to more graupel-sized hydrometeors at the expense of hail stones. However, once hail does form in polluted simulations, the large amounts of cloud water and ice available to be accreted can lead to rapid hail growth, and hence the hail is larger on average than in the clean scenario.

As explained above, the production of warm rain in polluted clouds is less efficient because of the larger numbers of smaller cloud drops in these clouds. Though the total convective precipitation in polluted simulations increases with increased aerosol loading because of the

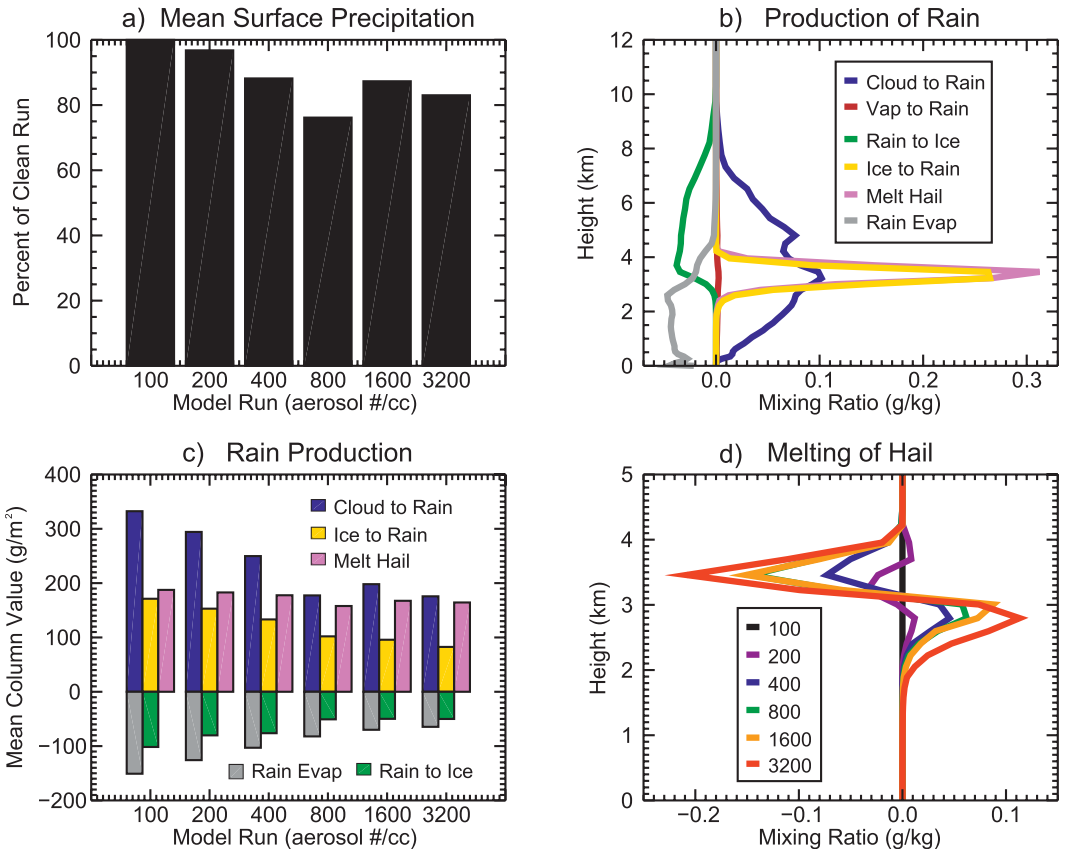

FIG. 4. (a) Mean surface precipitation, averaged over DCC profiles. Precipitation is plotted as a percentage of the clean (100 cm^{-3}) run. (b) Average profile of processes important to the production of rain in DCCs for the clean run. (c) Mean vertically integrated values of rain production terms in DCCs. Note the ''vap to rain'' term is small relative to the other terms and is left out of this plot. (d) Average mass of hail melted in DCCs, as a difference from the clean run.

increased number of DCCs, Fig. 4a demonstrates that the average surface DCC precipitation for each simulation (again, the average over all DCC profiles) has the opposite trend. The trend is nearly monotonic, with one outlier in the 800-cm^{-3} run. This simulation is discussed further at the end of this section.

Decreased precipitation with increased aerosol concentration is what has been typically found in previous studies concerning shallow clouds. However, it is not just collision and coalescence that acts to produce rain in DCCs—the ice phase is also an important consideration. The processes that contribute to the formation of rain are plotted for the clean run in Fig. 4b. ''Cloud to rain'' is the collision and coalescence of cloud drops to form raindrops—the warm rain process. ''Vapor to rain,'' a very small contribution compared to the others, consists of vapor diffusion onto raindrops. The production of rain by ice consists of two terms, ''ice to rain,'' the collection of ice by falling rain, and ''melt hail,'' the production of rain through the melting and shedding of hailstones. The melting of graupel does not directly contribute to precipitation in this model, as melted graupel is moved to the hail category (Meyers et al. 1997). Both of the terms involved in the production of rain associated with ice have large positive contributions to rain formation, but only in a very narrow layer near the freezing level. There are two sinks of rain. ''Rain to ice'' is the collection of rain by ice species, or the riming of rain, and ''rain evap'' is simply the evaporation of rain.

To examine the average column production of rain, each of the processes involved in producing rain was vertically integrated and averaged for the columns containing DCCs. The results are shown in Fig. 4c. The reduction in the warm rain process as a result of enhanced aerosol concentrations is quite clear, the reasons for which are described above. Because less rain is produced in polluted scenarios, there are fewer raindrops to collect ice particles as they fall, thus the ice to rain term also shows a significant reduction with

increased aerosols. The melt hail term decreases only slightly with increasing aerosols. Looking in more detail at the melting of hail (Fig. 4d), it becomes clear that rather than changing the amount of hail that is melted, an increase in aerosol concentration leads to a shift in where the melting is occurring. As explained above, even though hail mass is smaller in polluted simulations, the hail stones produced in polluted storms are able to grow larger because of the more abundant amounts of cloud water available for riming (Fig. 2). In the model, the melting and shedding of hail are accomplished using lookup tables. Hydrometeors of different sizes are given different fall speeds, and melting and shedding begin at the freezing level and continue as necessary until all of the hail is transferred to rain. Since the hail stones are larger in polluted storms, melting is less efficient and occurs through a deeper layer. Furthermore, in cleaner scenarios smaller hail is more easily transported to the anvil regions of the storms, and so less hail is available to melt and produce rain. The combination of these effects means that while total hail amount decreases significantly with increased aerosol concentration, the rain produced from the melting of hail only demonstrates a small change.

Also plotted in Fig. 4c are the sinks of rain, rain to ice and rain evap, both of which also decrease with increasing aerosol concentrations. Rain to ice, the removal of rain through riming, becomes less efficient as there is less mass of rain available to collect in the polluted simulations. The evaporation of rain also decreases with increasing aerosol concentration because the larger raindrops in polluted simulations are less efficient at evaporating.

A point to note from Fig. 4c is that the production of rain from ice (i.e., the sum of ice to rain and melt hail) is of the same magnitude or larger than that from warm rain production. As the background aerosol concentration increases and the warm rain production decreases, the production of rain through melting becomes increasingly important. Thus, enhanced aerosol concentrations lead to a shift in the importance of the processes contributing to rain production. Summing all of the terms in Fig. 4c reproduces the value for the average production of rain occurring within the DCCs. The average production of rain follows the trend of average surface precipitation seen in Fig. 4a, confirming that the reduction in precipitation can be explained. Though the production of rain in association with ice processes also decreases with increasing aerosol concentration, it is the decrease in warm rain production that dominates the trends seen in the average surface precipitation produced within the DCC profiles.

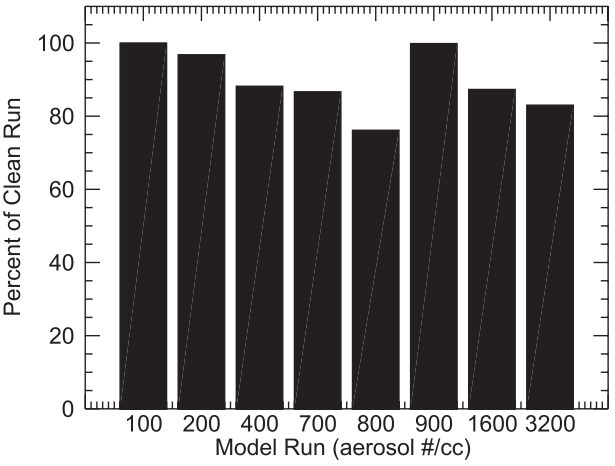

FIG. 5. As in Fig. 4a, but including the test simulations with aerosol concentrations of 700 and 900 cm^{-3}.

As described earlier, the 800-cm^{-3} simulation appears to be inconsistent when considering the trends in surface precipitation. To examine these inconsistencies, two additional simulations were completed with aerosol concentrations of 700 and 900 cm^{-3}. The goal was to investigate whether the 800-cm^{-3} run was an anomaly, or whether some kind of inflection point might exist near that value of aerosol concentration. Figure 5 shows the mean surface precipitation averaged over the DCCs, as plotted in Fig. 4a, but including the two additional simulations. The new simulations, with aerosol concentrations of 700 and 900 cm^{-3}, also demonstrate deviations from the overall precipitation trend. Trends in basic microphysical fields, such as number concentrations and diameters of hydrometeors, are robust throughout all of the simulations. This suggests that the physics are consistent, but that other factors such as the large-scale circulation or cold pool forcing, both of which are impacted by changes in aerosol concentrations, may play a role in these more moderate aerosol environments. We hypothesize that in this moderate aerosol regime, competing effects of microphysical processes as examined here, and dynamical processes such as cold pool interactions lead to variations in the overall response to increased aerosol concentrations. More work is necessary in order to examine this sensitivity; however, the overall differences between the cleanest simulations and the most polluted demonstrate the significant changes that occur because of aerosol impacts.

c. Updraft strength and convective invigoration

It has been demonstrated that changes in aerosol concentration lead to significant differences in storm microphysics and precipitation production. It follows that these differences may then feed back to the individual

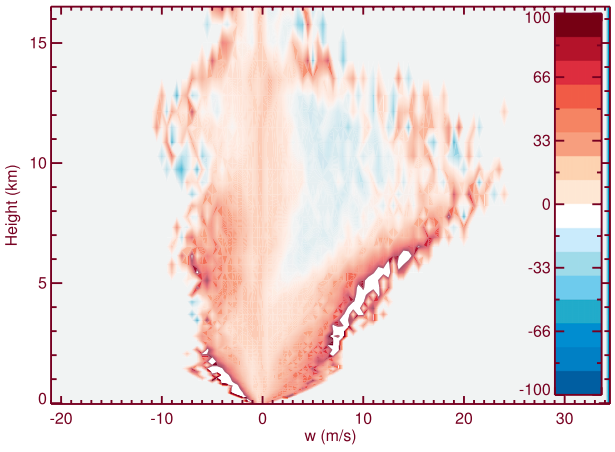

FIG. 6. Histogram of vertical velocity, displayed as a difference (in percentage of sample in DCCs) between the most polluted (3200 cm^{-3}) run and the clean run.

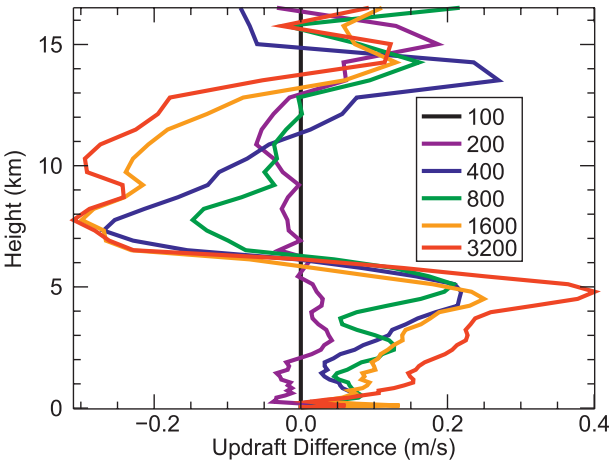

FIG. 7. Average updraft ($w > 1$ m s^{-1}) in DCCs, plotted as a difference from the clean run.

storm dynamics through changes in latent heating and thus updraft strength. Shown in Fig. 6 is a histogram displaying the frequency of occurrence of updraft and downdraft speeds as a function of height in DCCs. The frequency is normalized and then taken as a difference from the clean run, thereby demonstrating the change with increasing aerosol concentrations. Only one histogram is shown, but in each simulation with increasing aerosols, the same general trends can be seen. At any height, there is a shift toward more frequent occurrences of the strongest updraft and downdraft magnitudes in the more polluted scenarios, which is in agreement with the domainwide convective invigoration that was discussed in section 3a. In the lower levels (below about 6 km), this is a particularly clear trend—higher aerosols lead to stronger updrafts and downdrafts. In the upper levels, there is greater variation in vertical velocity, and the trend with increasing aerosols is more complex. There are generally more of the strongest and weakest updrafts in the polluted simulations at the expense of moderate (~5–15 m s^{-1}) updraft speeds, again, suggesting a shift toward more extreme values of vertical velocity.

A profile of average updraft velocity (updraft defined as those points with $w > 1$ m s^{-1}) is plotted in Fig. 7 as a difference from the clean run. Convective invigoration with increased aerosols can be seen clearly in the lower levels of the DCCs, up to about 6 km, and then the trend reverses and updrafts are weaker for higher values of aerosol loading. This trend reversal coincides with the increase in the variation of updraft speeds described above. The changes in updraft strength due to increasing aerosol concentration are more complex than suggested by Fig. 7, as looking at the average can mute out changes in the extreme values. Despite the increases in the stronger updraft speeds seen in the upper levels of the DCCs, changes in the moderate and lower values of updraft strength lead to the average updraft strength decreasing with increasing aerosol concentrations. Though the average value does not tell the whole story, the potential contributions to updraft changes will be examined in an average sense, so as to identify which processes are generally most important to convective invigoration trends evident over the whole sample of DCCs.

Previous studies that have seen convective invigoration (Andreae et al. 2004; Khain et al. 2005; van den Heever et al. 2006; Rosenfeld et al. 2008; Tao et al. 2012) have determined that the increase in updraft speed was brought about by an increase in the freezing of liquid cloud water to form ice. A budget of the processes included in the buoyancy term of the vertical velocity equation was undertaken here in order to examine in more detail how updraft speed is affected by pollution in this series of simulations. The vertical velocity equation is composed of three main terms: horizontal and vertical advection, the pressure gradient term, and buoyancy, all of which may be affected by the presence of aerosols. However, because this analysis has been limited to processes occurring within a single (DCC) column, and because the particular hypothesis being examined concerns latent heating, only the buoyancy term is examined here. The buoyancy term in the vertical velocity equation is shown below:

$$B = g\left(\frac{\theta'}{\theta_0}\right) - gq_c. \quad (1)$$

The buoyancy of a parcel B is affected by two terms, as shown in Eq. (1). Term 1 describes gravity g acting on a change in density brought about by a difference in

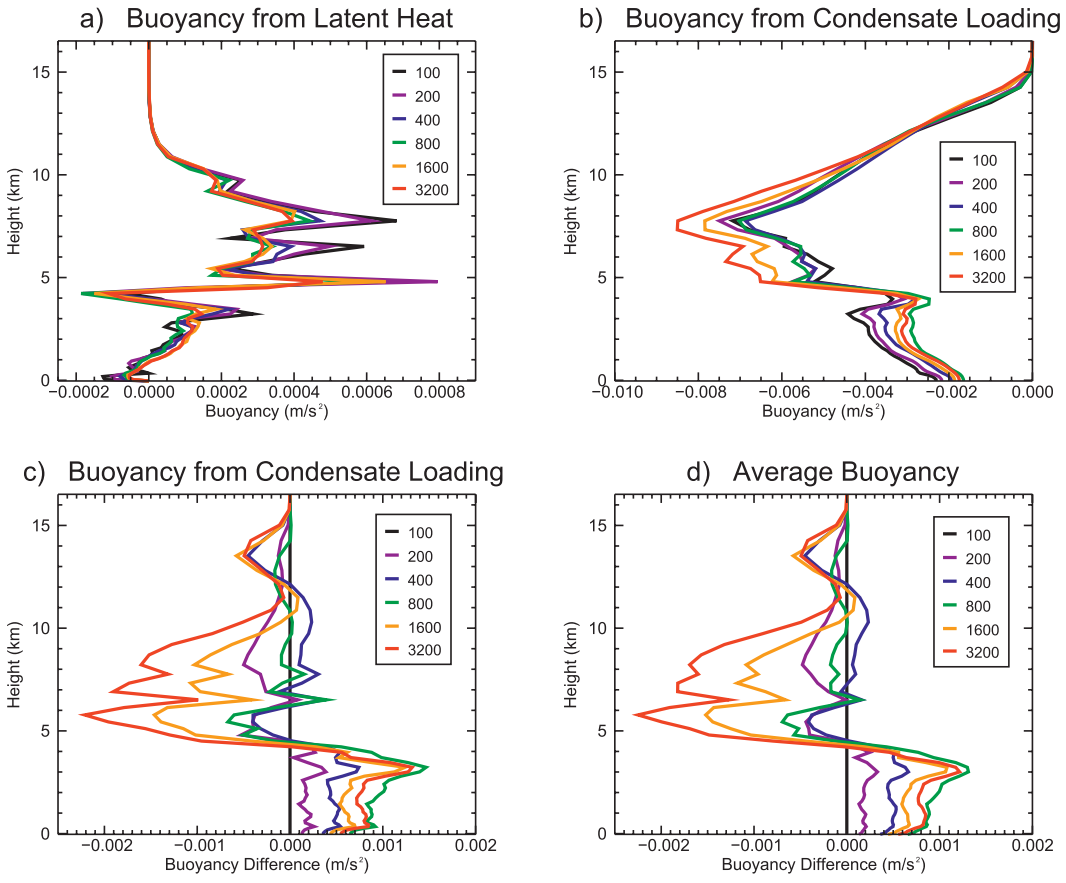

FIG. 8. (a) The increase in temperature due to latent heating [term 1 in Eq. (1)]. (b) Loss of buoyancy due to condensate loading [term 2 in Eq. (1)]. (c) The condensate loading term plotted as a difference from the clean run. The differences between simulations in this term are an order of magnitude larger than in term 1. (d) The total buoyancy as calculated in Eq. (1), plotted as a difference from the clean run. Terms are average profiles in DCCs.

potential temperature. In this equation, θ_0 is the mean, base-state potential temperature, and θ' is the difference in potential temperature brought about by latent heat release. Term 2 is the drag associated with the presence of liquid water and ice, or condensate loading, where q_c is the total condensate (liquid water + ice) mixing ratio.

Term 1 in Eq. (1), the buoyancy differences brought about by changes in potential temperature due to latent heat release, is plotted in Fig. 8a. There is a slight increase in latent heating with increased aerosols—up to about 3 km. The differences between the simulations become quite complex above that, however, as there are a number of processes that contribute. Figure 9 shows an average profile of the important contributions to latent heating for the cleanest and most-polluted runs. As stated earlier, theory of aerosol indirect effects suggests that freezing of additional cloud water leads to increased latent heat release, and hence convective invigoration (Andreae et al. 2004; Khain et al. 2005; Wang 2005; van den Heever et al. 2006; Rosenfeld et al. 2008; Tao et al. 2012). The freezing of liquid water can be represented by two terms plotted in Fig. 9: "ice nuc," the nucleation of ice particles, and "rime," the riming of liquid water onto existing ice particles. These two processes, represented by the yellow and pink lines in Fig. 9, respectively, are not relatively large contributions to the latent heating, regardless of the aerosol concentration. It can be seen in this example that the largest positive contributions to latent heating come from cloud nucleation, condensation, and depositional freezing, with the largest negative contributions coming from evaporation and sublimation. To see the impact of increased aerosols, these five most important processes are plotted for each simulation in Fig. 10.

In the initial stages of cloud development, polluted clouds undergo much more nucleation since there are more aerosols available to be activated as CCN. However, throughout most of the lifetime of the storms in polluted scenarios, condensation by vapor diffusion onto existing cloud drops becomes a much more dominant

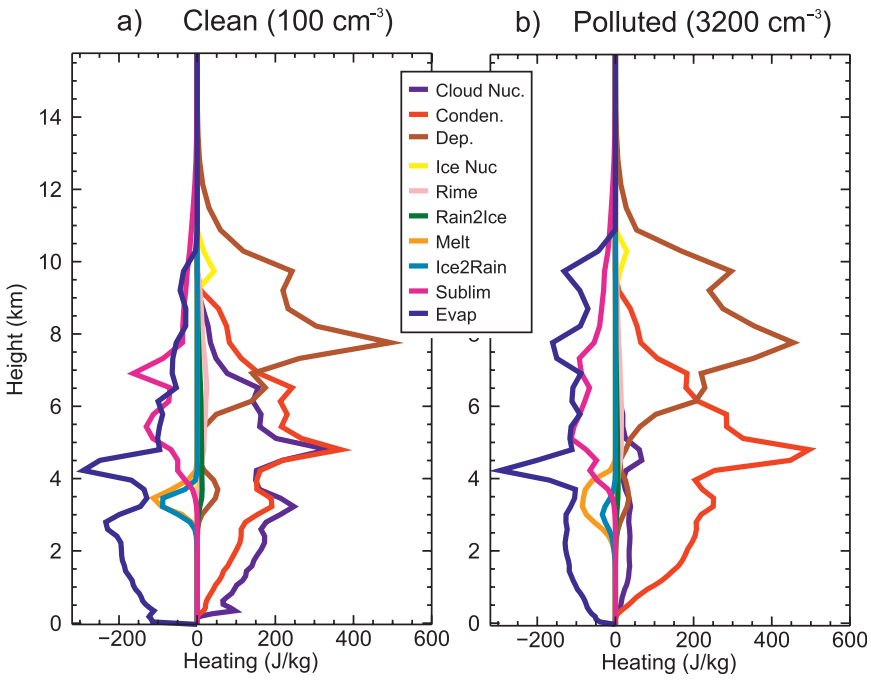

FIG. 9. Average profiles of latent heating processes in DCCs for (a) the clean (100 cm^{-3}) run and (b) the most polluted (3200 cm^{-3}) run.

process. This is due to the increased surface area associated with the presence of larger numbers of smaller drops. For a simple example, consider 1 m^3 of cloud containing 0.5 g of liquid water. In a clean scenario, the population of cloud drops may be 10 cm^{-3} and in a polluted case 100 cm^{-3} (see Fig. 2). If the liquid water is divided evenly among the cloud drop population (i.e., all drops are assumed to be the same size), the clean case has a cloud drop size of 22.9 μm and the polluted case 10.6 μm. By summing over the entire sample, the collective surface areas of the cloud drops would be 0.0656 and 0.141 m^2, respectively. There is roughly twice the surface area in the hypothetical polluted case, and since vapor diffusion onto cloud drops is proportional to surface area, the condensation would increase accordingly. Because there is so much competition for water vapor once such a population of cloud drops is established, new cloud drop nucleation becomes of secondary importance, as existing cloud droplets provide less of an energy barrier to condensation. Thus, when averaged over the lifetime of the DCCs, condensation shows a substantial increase with increasing aerosol concentration, while cloud nucleation decreases (Fig. 10). Other studies have shown similar increases in condensation with increased aerosol concentration (Khain et al. 2008; Lee et al. 2008a). The other important process that contributes greatly to positive latent heating in DCCs is deposition of vapor onto ice. This increases with increasing aerosol concentrations because of the fact that there is a greater mass of cloud ice and most of the cloud ice is in the form of more numerous, smaller aggregates (not shown). Thus, the same surface area effect occurs for depositional freezing as was just described for condensation.

Acting to balance the positive contributions to latent heating are evaporation and sublimation (Fig. 10). Evaporation in cloud shows a distinct increase with increasing aerosol concentrations owing to the smaller cloud drops, which evaporate more easily. Evaporation is also seen to occur at higher elevations in polluted DCCs because of the presence of small cloud drops, which can be lofted higher in the clouds. However, in the lower levels, evaporation actually decreases with increasing aerosol concentrations, since in this region of the cloud and below, evaporation of rain is more dominant than evaporation of cloud water, and as discussed earlier, the raindrops are larger (Fig. 2) and thus less efficient at evaporating. Sublimation decreases with increasing aerosols, which is counter to what occurs with evaporation. Increased evaporation in cloud leads to more instances of ice supersaturation, which enhances deposition onto ice through the Bergeron–Findeisen process, so sublimation is less likely to occur in the more polluted scenarios.

The processes contributing to buoyancy through latent heating do not, by themselves, explain the trend

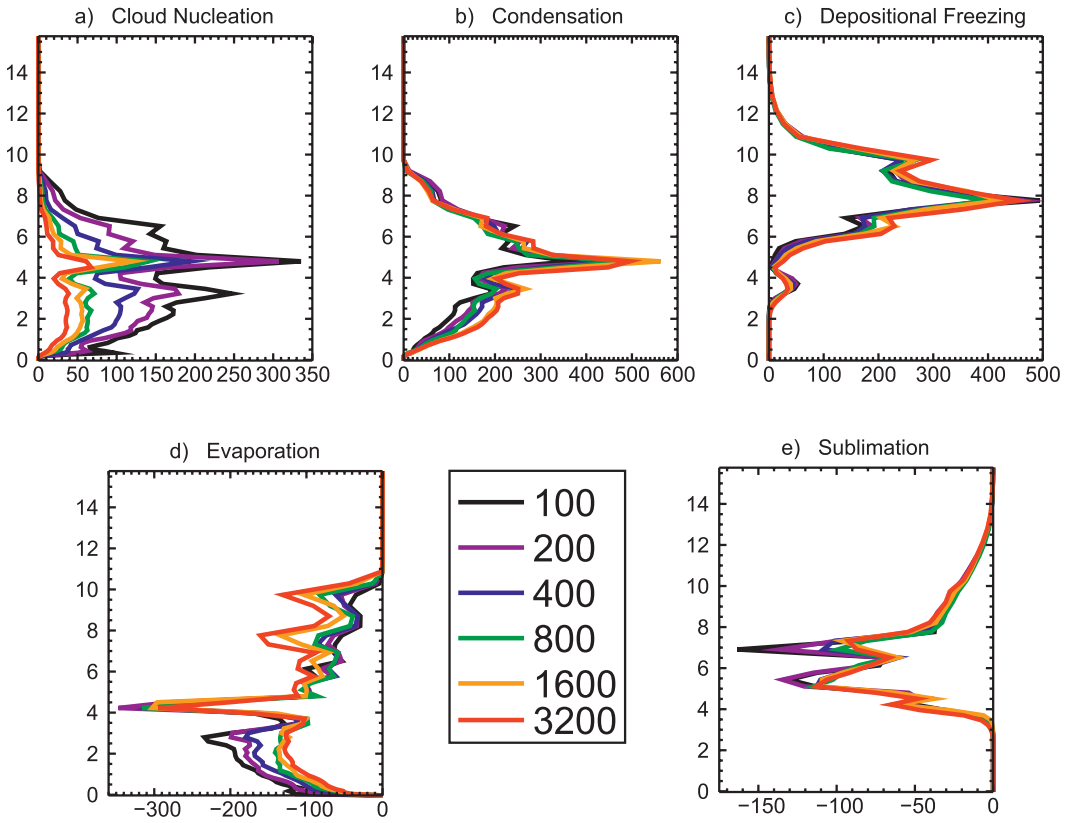

FIG. 10. Average profiles of the mass produced by (a) cloud nucleation, (b) condensation, (c) depositional freezing, (d) evaporation, and (e) sublimation, the most important processes involved in latent heat release in DCCs. Units are mixing ratio (g kg^{-1}).

seen in the mean updraft. In the lower levels, an increase in buoyancy can be seen largely because of decreased rain evaporation (i.e., reduced evaporational cooling leads to comparatively warmer air near the surface, which will be more buoyant), but there is no clear link between the latent heating term and the decreased updraft speed above 6 km. To further explain this, it is necessary to look at the condensate loading term in Eq. (1). Figure 8b shows the condensate loading as a function of aerosol concentration, where the condensate loading is simply the weight of the liquid water and ice contained within the DCCs. In polluted storms, more liquid and ice exist within cloud (Fig. 3), leading to a much larger drag on the updraft from the weight of the condensate. Though the heating and condensate terms themselves (Fig. 8a and b) are of comparable magnitude, the differences between the simulations are much larger in the condensate loading term (Fig. 8c), and as such dominate the trends in total buoyancy above 6 km (Fig. 8d). The large change in condensate loading leads to a decrease in buoyancy, and hence contributes to the decreased (average) updraft speed with increased aerosols above 6 km.

The shape of the average updraft profile (Fig. 7) is well approximated by the buoyancy term, as shown in Fig. 8d. This suggests that the buoyancy term is a large factor in determining the difference in average updraft speed with increased aerosol concentrations. Clear convective invigoration can be seen below the freezing level, where increases in condensation, decreases in evaporation, and decreases in condensate loading all act together to produce increased buoyancy in the polluted simulations. Above this, the condensate loading term dominates, and so the average updraft decreases with increasing aerosol concentrations. However, again it must be pointed out that the average value is not always representative of all of the changes that are occurring. As shown in Fig. 6, the upper levels do contain more extreme values of vertical velocity, along with a reduction in the frequency of the more moderate updraft strengths, which is consistent with convective invigoration. The vertical velocity profile within each DCC relies upon a balance between condensate loading and the various processes involved in latent heating. The histogram of vertical velocity is consistent with the domainwide statistics. The convective circulation is invigorated with increased aerosol

concentrations; however, not every DCC shows the same response, and enough of the DCC profiles are weighed down by the excess condensate produced that the average updraft speed decreases with increasing aerosol concentration.

It has been asserted by previous studies that convective invigoration would be brought about by additional latent heat released in the freezing of cloud water. This study does show that increases in latent heating, especially below 6 km, can lead to increased updraft strength and convective invigoration. There are many processes that contribute to these changes in latent heating; particularly important are condensation and vapor deposition onto ice. The stronger updrafts seen in the early stages of convection were invigorated with increased aerosol concentrations. However, the weaker to moderate updrafts seen in more mature convection became weaker in polluted simulations owing to the effects of condensate loading, and led to the average updraft strength above 6 km decreasing with increased aerosol concentrations. It must be noted that the buoyancy term is just one term in the vertical velocity equation, and other possible dynamic feedbacks such as cold pools have not been examined here. When considering processes contributing to convective invigoration, this study concludes that condensation and vapor diffusion onto ice are of great importance and the drag associated with condensate loading must be considered as well.

4. Conclusions

A series of large-scale, two-dimensional RCE model simulations has been used to demonstrate that significant differences in microphysics, dynamics, and large-scale organization of DCCs develop from differences in background aerosol concentration. The basic warm cloud microphysical differences were shown to follow the traditional predictions of the first and second aerosol indirect effects, but in order to more fully explain changes in surface precipitation amount and updraft speed in DCCs, it was necessary to involve ice-phase microphysics in the analysis. The ice-phase microphysics was investigated using a detailed examination of the microphysical processes involved in the production of precipitation and the generation of buoyancy.

Over the whole domain, the number of deep convective storms increased in number and size with increasing aerosol concentrations. Domainwide cloud-top counts showed a shift toward more high cloud tops and fewer low cloud tops, suggesting an invigoration of the DCCs when aerosol loading was increased. Additionally, the total deep convective precipitation increased with increasing aerosols, and it also made up a larger percentage of the total domainwide precipitation total. This suggests that the large-scale convective circulations were stronger in the polluted simulations, with increased convective mass flux in the moist bands, and enhanced subsidence in the surrounding regions.

Though the total domainwide convective precipitation increased with increasing aerosol concentration, the average precipitation produced by each DCC decreased. This was due to a combination of factors. The warm rain process in the polluted simulations was less effective because of the smaller cloud drop sizes. The production of rain through ice processes (melting of hail and riming of rain) also decreased with increasing aerosols, but the warm rain reduction was the dominant term in determining the average precipitation trend. However, as the background aerosol concentration increased, the production of rain through the melting of ice became relatively more important. It should be noted that some precipitation was likely produced in the stratiform anvil regions associated with the DCCs studied here, which was not included in this analysis, but would add to the convective precipitation total. In general, the results presented here suggest that ice-phase microphysics can become increasingly important for deep convective storms as aerosol concentrations increase.

Looking in more detail at the updrafts in polluted storms, it was seen that the DCCs formed in polluted simulations were more likely to have stronger updrafts and downdrafts; however, above 6 km the frequency of moderate updrafts decreased, while those of the weaker and stronger updrafts increased, thus leading to an overall decrease in the average updraft strength. In other words, there were more intense storms, but also more weak updrafts, in polluted cases. Previous studies that noted convective invigoration with increasing aerosols attributed the change in updraft speed to increases in latent heat from the freezing of a larger mass of cloud water. To examine that theory, the buoyancy term in the vertical velocity was examined in detail. In polluted storms, increased latent heat was released in the freezing of cloud water to form ice, and even more so from condensation and vapor diffusion processes (both onto liquid water and ice). However, in addition to the enhanced latent heat release, the larger ice amounts produced in polluted storms served to increase the condensate loading of the updraft, which ultimately reversed the trend in buoyancy above the freezing level, contributing to the decrease in average updraft speed above 6 km. It should be noted that the buoyancy term is not the only possible way that vertical velocity may have been affected by aerosol concentrations. For example, changes in near-surface evaporation will affect the

strength of cold pools produced by convective storms, which can in turn impact new convection [as seen in van den Heever and Cotton (2007); Storer et al. (2010)]. However, the results of this study demonstrate the importance of considering the variety of microphysical processes that contribute to latent heating within DCCs, and also demonstrate the importance of condensate loading as a factor that can influence how aerosols affect updraft strength.

The buoyancy term calculated herein appeared to play a significant role in effecting changes in vertical velocity with increased aerosol concentration. Increases in updraft speed in the lower levels of the DCCs examined (below about 5 km) can be attributed to a combination of increases in condensation, decreases in evaporation, and decreases in condensate loading. Above this height, the average buoyancy term was dominated by increases in condensate loading in polluted simulations, leading to a decrease in the average updraft speed in these levels. However, histograms of vertical velocity demonstrated increased occurrences of the more extreme values at the expense of moderate values. This, along with the strong domainwide trends, does suggest that convective invigoration was occurring, with some of the DCCs being affected by the mechanisms of convective invigoration predicted by previous studies (Andreae et al. 2004; Khain et al. 2005; Wang 2005; van den Heever et al. 2006; Rosenfeld et al. 2008; Koren et al. 2010; Li et al. 2012; Tao et al. 2012) in order to bring about the domainwide invigoration of the large-scale convective circulations (more and larger storms, higher cloud tops, increased total precipitation). However, the actual updraft profile of each DCC was shown to depend on a precarious balance between condensate loading, evaporation, condensation, vapor deposition, and the many other processes involved in latent heating throughout the clouds. The enhanced frequency of stronger updrafts and the reduced frequency of more moderate updrafts within more polluted environments lead us to speculate that the effect of aerosol concentrations on DCC updrafts has a lifetime dependence; that is, early in the life cycle of deep convective storms, latent heating changes are dominant, leading to stronger updrafts, higher cloud tops, and more horizontally developed storms, whereas updrafts occurring during the more mature and dissipating phase of storm lifetime are more likely to be weighed down by increased condensate loading.

It has been demonstrated in this study that surface precipitation, storm strength, and larger-scale convective organization can all be affected by changing the number of aerosols available to act as CCN. Many questions regarding aerosol indirect effects on deep convective clouds and other cloud types remain unanswered though. For instance, aerosols can also serve as ice nuclei or GCCN, possibly leading to competing effects that require further study. Future work will entail comparisons with satellite observations (such as *CloudSat*), and a detailed examination of how the microphysical budgeting terms change throughout the lifetime of a DCC in order to gain a more complete picture of how aerosols can affect deep convective storms.

Acknowledgments. This work was funded by the National Science Foundation under Grant NSFATM-0820557. The authors thank Steven M. Saleeby for providing the microphysical budgeting code for RAMS. Thanks also to the three anonymous reviewers, whose useful comments have added to the quality of this manuscript.

REFERENCES

Albrecht, B., 1989: Aerosols, cloud microphysics, and fractional cloudiness. *Science,* **245,** 1227–1230.

Altaratz, O., I. Koren, and T. Reisin, 2007: Aerosols' influence on the interplay between condensation, evaporation and rain in warm cumulus cloud. *Atmos. Chem. Phys.,* **7,** 12 687–12 714.

Andreae, M., D. Rosenfeld, P. Artaxo, A. Costa, G. Frank, K. Longo, and M. Silva-Dias, 2004: Smoking rain clouds over the Amazon. *Science,* **303,** 1337–1342.

Arakawa, A., 2004: The cumulus parameterization problem: Past, present, and future. *J. Climate,* **17,** 2493–2525.

Berg, W., T. L'Ecuyer, and S. van den Heever, 2008: Evidence for the impact of aerosols on the onset and microphysical properties of rainfall from a combination of satellite observations and cloud-resolving model simulations. *J. Geophys. Res.,* **113,** D14S23, doi:10.1029/2007JD009649.

Bretherton, C., P. Blossey, and M. Khairoutdinov, 2005: An energy-balance analysis of deep convective self-aggregation above uniform SST. *Rev. Geophys.,* **62,** 4273–4292.

Carlson, T. N., and J. M. Prospero, 1972: The large-scale movement of Saharan air outbreaks over the northern equatorial Atlantic. *J. Appl. Meteor.,* **11,** 283–297.

Cotton, W., and Coauthors, 2003: RAMS 2001: Current status and future directions. *Meteor. Atmos. Phys.,* **82,** 5–29.

Demott, P. J., K. Sassen, M. R. Poellot, D. Baumgardner, D. C. Rogers, S. D. Brooks, A. J. Prenni, and S. M. Kreidenweis, 2003: African dust aerosols as atmospheric ice nuclei. *Geophys. Res. Lett.,* **30,** 1732, doi:10.1029/2003GL017410.

Fan, J., R. Zhang, G. Li, and W.-K. Tao, 2007: Effects of aerosols and relative humidity on cumulus clouds. *J. Geophys. Res.,* **112,** D14204, doi:10.1029/2006JD008136.

——, and Coauthors, 2009: Dominant role by vertical wind shear in regulating aerosol effects on deep convective clouds. *J. Geophys. Res.,* **114,** D22206, doi:10.1029/2009JD012352.

Feingold, G., S. Tzivion, and Z. Leviv, 1988: Evolution of raindrop spectra. Part I: Solution to the stochastic collection/breakup equation using the method of moments. *J. Atmos. Sci.,* **45,** 3387–3399.

——, R. Walko, B. Stevens, and W. Cotton, 1998: Simulations of marine stratocumulus using a new microphysical parameterization scheme. *Atmos. Res.,* **47–48,** 505–528.

Fierro, A. O., J. Simpson, M. A. LeMone, J. M. Straka, and B. F. Smull, 2009: On how hot towers fuel the Hadley cell: An observational and modeling study of line-organized convection in the equatorial trough from TOGA COARE. *J. Atmos. Sci.,* **66,** 2730–2746.

——, E. J. Zipser, M. A. LeMone, J. M. Straka, and J. M. Simpson, 2012: Tropical oceanic hot towers: Need they be undilute to transport energy from the boundary layer to the upper troposphere effectively? An answer based on trajectory analysis of a simulation of a TOGA COARE convective system. *J. Atmos. Sci.,* **69,** 195–213.

Grabowski, W. W., 2006: Indirect impact of atmospheric aerosols in idealized simulations of convective–radiative quasi equilibrium. *J. Climate,* **19,** 4664–4682.

Harrington, J., T. Reisin, W. Cotton, and S. Kreidenweis, 1999: Cloud resolving simulations of Arctic stratus Part II: Transition-season clouds. *Atmos. Res.,* **51,** 45–75.

Haynes, J., and G. Stephens, 2007: Tropical oceanic cloudiness and the incidence of precipitation: Early results from CloudSat. *Geophys. Res. Lett.,* **34,** L09811, doi:10.1029/2007GL029335.

Held, I. M., R. S. Hemler, and V. Ramaswamy, 1993: Radiative convective equilibrium with explicit two-dimensional moist convection. *J. Atmos. Sci.,* **50,** 3909–3927.

Johnson, R. H., T. M. Rickenbach, S. A. Rutledge, P. E. Ciesielski, and W. H. Schubert, 1999: Trimodal characteristics of tropical convection. *J. Climate,* **12,** 2397–2418.

Karyampudi, V. M., and Coauthors, 1999: Validation of the Saharan dust plume conceptual model using lidar, Meteosat, and ECMWF data. *Bull. Amer. Meteor. Soc.,* **80,** 1045–1075.

Khain, A., 2009: Notes on state-of-the-art investigations of aerosol effects on precipitation: A critical review. *Environ. Res. Lett.,* **4,** 015004, doi:10.1088/1748-9326/4/1/015004.

——, D. Rosenfeld, and A. Pokrovsky, 2005: Aerosol impact on the dynamics and microphysics of deep convective clouds. *Quart. J. Roy. Meteor. Soc.,* **131,** 2639–2664.

——, N. BenMoshe, and A. Pokrovsky, 2008: Factors determining the impact of aerosols on surface precipitation from clouds: An attempt at classification. *J. Atmos. Sci.,* **65,** 1721–1748.

Koren, I., G. Feingold, and L. A. Remer, 2010: The invigoration of deep convective clouds over the Atlantic: Aerosol effect, meteorology or retrieval artifact? *Atmos. Chem. Phys.,* **10,** 8855–8872, doi:10.5194/acp-10-8855-2010.

Lebsock, M. D., G. L. Stephens, and C. Kummerow, 2008: Multisensor satellite observations of aerosol effects on warm clouds. *J. Geophys. Res.,* **113,** D15205, doi:10.1029/2008JD009876.

Lee, S. S., L. J. Donner, V. T. J. Phillips, and Y. Ming, 2008a: Examination of aerosol effects on precipitation in deep convective clouds during the 1997 ARM summer experiment. *Quart. J. Roy. Meteor. Soc.,* **134,** 1201–1220.

——, ——, ——, and ——, 2008b: The dependence of aerosol effects on clouds and precipitation on cloud-system organization, shear and stability. *J. Geophys. Res.,* **113,** D16202, doi:10.1029/2007JD009224.

Li, Z., F. Niu, J. Fan, Y. Liu, D. Rosenfeld, and Y. Ding, 2012: Long-term impacts of aerosols on the vertical development of clouds and precipitation. *Nat. Geosci.,* **4,** 888–894, doi:10.1038/ngeo1313.

Liu, C., 2011: Rainfall contributions from precipitation systems with different sizes, convective intensities, and durations over the tropics and subtropics. *J. Hydrometeor.,* **12,** 394–412.

May, P. T., V. N. Bringi, and M. Thurai, 2011: Do we observe aerosol impacts on DSDs in strongly forced tropical thunderstorms? *J. Atmos. Sci.,* **68,** 1902–1910.

Meyers, M., R. Walko, J. Harrington, and W. Cotton, 1997: New RAMS cloud microphysics parameterization. Part II: The two-moment scheme. *Atmos. Res.,* **45,** 3–39.

Pielke, R., W. Cotton, R. Walko, and C. Tremback, 1992: A comprehensive meteorological modeling system—RAMS. *Meteor. Atmos. Phys.,* **49,** 69–91.

Posselt, D. J., S. C. van den Heever, and G. L. Stephens, 2008: Trimodal cloudiness and tropical stable layers in simulations of radiative convective equilibrium. *Geophys. Res. Lett.,* **35,** L08802, doi:10.1029/2007GL033029.

Rickenbach, T., and S. Rutledge, 1998: Convection in TOGA COARE: Horizontal scale, morphology, and rainfall production. *J. Atmos. Sci.,* **55,** 2715–2729.

Riehl, H., and J. S. Malkus, 1958: On the heat balance in the equatorial trough zone. *Geophysica,* **6,** 503–538.

Rose, D., and Coauthors, 2010: Cloud condensation nuclei in polluted air and biomass burning smoke near the mega-city Guangzhou, China—Part 1: Size-resolved measurements and implications for the modeling of aerosol particle hygroscopicity and CCN activity. *Atmos. Chem. Phys.,* **10,** 3365–3383.

Rosenfeld, D., and I. Lensky, 1998: Satellite-based insights into precipitation formation processes in continental and maritime convective clouds. *Bull. Amer. Meteor. Soc.,* **79,** 2457–2476.

——, U. Lohmann, G. Raga, C. O'Dowd, M. Kulmala, S. Fuzzi, A. Reissell, and M. Andreae, 2008: Flood or drought: How do aerosols affect precipitation? *Science,* **321,** 1309–1313.

Saleeby, S., and W. Cotton, 2004: A large-droplet mode and prognostic number concentration of cloud droplets in the Colorado State University Regional Atmospheric Modeling System (RAMS). Part I: Module descriptions and supercell test simulations. *J. Appl. Meteor.,* **43,** 182–195.

Seifert, A., and K. Beheng, 2006: A two-moment cloud microphysics parameterization for mixed-phase clouds. Part 2: Maritime vs. continental deep convective storms. *Meteor. Atmos. Phys.,* **92,** 67–82.

Solomon, S., and Coauthors, 2007: Technical summary. *Climate Change 2007: The Physical Science Basis,* S. Solomon et al., Eds., Cambridge University Press, 19–91.

Stephens, G. L., S. van den Heever, and L. Pakula, 2008: Radiative–convective feedbacks in idealized states of radiative–convective equilibrium. *J. Atmos. Sci.,* **65,** 3899–3916.

Storer, R. L., S. C. van den Heever, and G. L. Stephens, 2010: Modeling aerosol impacts on convective storms in different environments. *J. Atmos. Sci.,* **67,** 3904–3915.

Tao, W.-K., J.-P. Chen, Z. Li, C. Wang, and C. Zhang, 2012: Impact of aerosols on convective clouds and precipitation. *Rev. Geophys.,* **50,** RG2001, doi:10.1029/2011RG000369.

Tompkins, A. M., and G. C. Craig, 1998: Radiative–convective equilibrium in a three-dimensional cloud-ensemble model. *Quart. J. Roy. Meteor. Soc.,* **124,** 2073–2097.

Twohy, C. H., and Coauthors, 2009: Saharan dust particles nucleate droplets in eastern Atlantic clouds. *Geophys. Res. Lett.,* **36,** L01807, doi:10.1029/2008GL035846.

Twomey, S., 1977: The influence of pollution on the shortwave albedo of clouds. *J. Atmos. Sci.,* **34,** 1149–1152.

van den Heever, S. C., 2011: The impacts of aerosol indirect forcing on dynamical aspects of deep convection. Extended Abstracts, *Fall Meeting,* San Francisco, CA, Amer. Geophys. Union, A13G-03.

——, and W. R. Cotton, 2007: Urban aerosol impacts on downwind convective storms. *J. Appl. Meteor. Climatol.,* **46,** 828–850.

——, G. G. Carrió, W. R. Cotton, P. J. DeMott, and A. J. Prenni, 2006: Impacts of nucleating aerosol on Florida storms. Part I: Mesoscale simulations. *J. Atmos. Sci.,* **63,** 1752–1775.

——, G. L. Stephens, and N. B. Wood, 2011: Aerosol indirect effects on tropical convection characteristics under conditions of radiative–convective equilibrium. *J. Atmos. Sci.,* **68,** 699–718.

Walko, R., and Coauthors, 2000: Coupled atmosphere–biophysics–hydrology models for environmental modeling. *J. Appl. Meteor.,* **39,** 931–944.

Wang, C., 2005: A modeling study of the response of tropical deep convection to the increase of cloud condensation nuclei concentration: 1. Dynamics and microphysics. *J. Geophys. Res.,* **110,** D21211, doi:10.1029/2004JD005720.

Zipser, E. J., and Coauthors, 2009: The Saharan air layer and the fate of African easterly waves—NASA's AMMA field study of tropical cyclogenesis. *Bull. Amer. Meteor. Soc.,* **90,** 1137–1156.